J Therm Anal Calorim
DOI 10.1007/s10973-016-5680-7

Structural characterization and thermal behaviour of some azomethine compounds derived from pyridoxal and 4-aminoantipyrine

Réka-Ştefana Mezey[1] · Traian Zaharescu[2] · Marius Eduard Lungulescu[2] · Virgil Marinescu[2] · Sergiu Shova[3] · Tudor Roşu[1]

Received: 17 January 2016 / Accepted: 30 June 2016

Abstract Eight azomethine-type compounds (**1**–**8**) derived from pyridoxal (3-hydroxy-5-(hydroxymethyl)-2-methylpyridine-4-carbaldehyde) and 4-aminoantipyrine, respectively, were prepared and thoroughly characterized from structural and thermal perspective. The structures of the compounds were studied based on IR, ^{1}H and ^{13}C NMR spectroscopy and electrospray ionization mass spectrometry. The formation of the azomethine derivatives is confirmed by the occurence of signals typical for the imine bond. Compounds **6** and **8** feature a high crystallinity, and their structures were resolved by single-crystal X-ray diffraction. The thermal behaviour of all the compounds was studied by non-isothermal chemiluminescence in static air atmosphere at different heating rates. The pattern of the oxidation process is described. Moreover, thermo-gravimetric and differential scanning calorimetry experiments were conducted in order to assess the thermal oxidation stability. The onset oxidation temperatures show a high thermal stability for all the tested azomethine compounds. The crystallinity degree was comparatively evaluated on the basis of melting enthalpy values and discussed in connection with the molecular structure. Compounds **6**–**8** show the higher thermal stability and crystallinity degree.

Keywords Azomethine compounds · Pyridoxal · 4-Aminoantipyrine · Thermal studies · Crystal structure

Introduction

The azomethine compounds as well as their transition metal complexes represent a field of high interest for both inorganic chemistry and biochemistry due to their pharmacological effects [1–4]. The key element of the azomethine compounds is the imine bond which was connected with a series of chemical and pharmacological properties. In particular, due to their easy preparation and high stability, this category of compounds contributes to the development of coordinative chemistry by serving as excellent ligands for the transitional metal ions. Since the imine bond containing molecules are versatile and possess electron donor properties, they are able to facilely coordinate to the metal ions via the nitrogen atom of the azomethine bond. In addition, if the ligand molecule posses other functional moieties suitable for coordination (like –OH, –SH, $–NO_2$) close enough to the azomethine group, the probability to obtain mono- or polychelates rings with increased kinetic and thermodynamic stability is very high [5, 6]. Several such complexes derived from azomethine ligands not only exhibit a superior pharmacological effect—antimicrobial, anti-inflammatory and analgesic—compared to the free ligand, but also a high thermal stability [7, 8].

Starting from these considerations, there are favourable perspectives to emphasize the development of new organic compounds for further use as basis for the extension of

Electronic supplementary material The online version of this article (doi:10.1007/s10973-016-5680-7) contains supplementary material, which is available to authorized users.

✉ Réka-Ştefana Mezey
reka.mezey@gmail.com

[1] Department of Inorganic Chemistry, Faculty of Chemistry, University of Bucharest, 23 Dumbrava Rosie, 050107 Bucharest, Romania

[2] INCDIE ICPE CA, 313 Splaiul Unirii, 030138 Bucharest, Romania

[3] Institute of Macromolecular Chemistry "Petru Poni", 41A Grigore Ghica Voda, 400786 Iasi, Romania

Published online: 14 July 2016

application in metal complexes field. The full detailed characterization of new metal complex structures is mandatory to qualify the preparation and properties of these foreseen complexes. Turkyilmaz et al. [9] synthesized, structurally characterized Cu(II), Ni(II) and Pt(II) azomethine polychelate complexes and identified certain thermal intervals of stability as well as the thermodynamic effects which accompany complexes degradation. The thermal decomposition pattern provides valuable information about the presence of smaller fragments (like H_2O molecule, Cl_2, inorganic anions) additioned to the metal complexes and about their position inside or outside of the coordination sphere [10]. Moreover, Zayed et al. [11] showed that the start decomposition temperature depends mainly on the instability of the non-coordinated terminal aliphatic parts of the ligand, while the decomposition temperature of the remaining fragment is connected with the affinity of the metal ion to the organic ligand.

The efficacy of each novel metal complex is highly dependent either on the electronic or on the structural properties of the involved ligands [10]. Ideally, the organic compounds should possess specific thermal and structural stability. For particular applications, the proper understanding of the behaviour of ligands is helpful for the explanation of the mechanism followed under different employment conditions [12, 13]. At the same time, because ligands are intermediates in the metal complex synthesis, the evaluation of their stability is of a great importance for the selection of proper conditions for preparation. At the same time, the interference of degrading secondary compounds can be significantly diminished.

The thermal, thermo-oxidative and thermo-gravimetric methods are background procedures for the characterization of complexes stability and their thermodynamic parameters [12, 14, 15]. Several studies analyse the thermodynamic parameters for complexes in connection with the TG–DTG curves and decomposition model [16]. For several metal complexes with ligand 2-benzoyl-pyridil-isonicotinoylhydrazone, the decomposition heats and ΔH associated with the exothermal effects were determined [17]. Abdel-Fattah et al. [18] used the information provided by the DTG curves in order to determine the kinetic reaction order of the decomposition of several Schiff base complexes as well as to calculate the activation entropy, activation enthalpy and free energy of activation correlated with the thermal stability.

While the academic research is focused on the evaluation of physical and thermal properties of metal complexes, a real interest to the characterization of the uncoordinated ligands was scarcely observed. In order to add valuable information to the field of azomethine compounds, we characterized some imine structures derived from pyridoxal and 4-aminoantipyrine, respectively. They are foreseen to be used for the preparation of transition metal complexes with pharmacological effects. The selection of these compounds for the synthesis of azomethine compounds is connected with their biological properties. Pyridoxal is one of the five naturally interconvertible forms of vitamin B_6 which exhibits a large spectrum of applications in the field of medicine, including its role in the metabolic decarboxylation and transamination of amino acids [19], the coenzymatic effect in many biological processes [20] and the antioxidant capacity [21]. Many of the biomechanisms which depend on pyridoxal involve the formation of an azomethine intermediate. On the other hand, pyridoxal could induce tuning of the electronic properties of the azomethine ligands and their corresponding complexes by protonation–deprotonation of the heterocyclic nitrogen atom due to the aldehyde group attached to the pyridine ring [22].

An extensive number of reports concerning antipyrine and its derivatives as antiviral, antimicrobial, antitumor and analgesic effects agents are available [23–26]. The antipyrine-derived complexes are also known for their high stability [12, 14, 27].

On this direction, the goals of this study are the synthesis and the detailed structural and thermal characterization of some compounds belonging to the azomethine category. The structural characterization of all compounds has been accomplished by elemental analysis, IR, ^{1}H and ^{13}C NMR spectroscopy and mass spectrometry. In addition, the crystal structures of two compounds are reported. Single-crystal X-ray diffraction was used as an accurate method to characterize the supramolecular systems generated by hydrogen bonds and aromatic π–π stacking interactions. The thermal stability is qualified by chemiluminescence, TG and DSC investigations, which provide basic information on the further behaviour of complexes in which they will be used. Keeping in mind, the use of these compounds as intermediates in the development of complex molecules, an extensive study concerning their thermal and thermo-oxidative properties, was conducted.

Experimental

Materials

Pyridoxal hydrochloride, 4-aminoantipyrine, phenylhydrazine hydrochloride, 2,4-dinitro-phenylhydrazine, 3-hydroxybenzoic acid hydrazide, 4-phenyl-3-thiosemicarbazide, 4-benzyl-3-thiosemicarbazide, 4-acetoxy-3-methoxybenzaldehyde, 3-benzyloxy-4-methoxybenzaldehyde and 4-(dimethylamino)benzaldehyde with high purity were purchased from Sigma-Aldrich and used as such without any further purification step.

Synthesis of the azomethine compounds

All the azomethine compounds have been synthesized by direct condensation reaction. The pyridoxal-derived compounds were obtained by condensation of the named substance with the corresponding hydrazine, hydrazide and thiosemicarbazide, in a 1:1 molar ratio. The second category of azomethine products have been prepared by 1:1 condensation of 4-aminoantipyrine with the carbonylic reagents.

*Pyridoxal-phenylhydrazone (**1**)*

A solution of 0.145 g (1 mmol) of phenylhydrazine hydrochloride in methanol (5 mL) was added slowly to a solution of 0.204 g (1 mmol) of pyridoxal hydrochloride in the same solvent (5 mL). The mixture was alkalized to pH = 7–7.5 by adding few drops of triethylamine (TEA) and constantly controlling the pH value. The reaction solution was stirred at 50 °C. After 30 min, a light yellow solid mass appeared. The mixture was keep stirring for another hour until the entire azomethine compound precipitated quantitatively. Further, it was filtered, washed with methanol and dried in vacuum. As a second step, the precipitate was purified by recrystallization. Reaction yield: 72 %. ESI-MS (positive mode, MeOH:H_2O) *m/z*: $[LH]^+$ calculated for $C_{14}H_{16}N_3O_2$ 258.30, found 259.00.

*Pyridoxal-2,4-dinitro-phenylhydrazone (**2**)*

To a solution of 0.204 g (1 mmol) of pyridoxal hydrochloride in methanol was added the methanolic solution of 0.198 g (1 mmol) of 2,4-dinitro-phenylhydrazine. A red–orange solution was formed immediately. A small amount of TEA was added to increase the pH of the solution to 7. The final solution was refluxed at controlled temperature (50 °C) for 1 h until a fine orange precipitate was isolated. The resulted mass was filtered, washed with alcohol and dried. The purity of the synthesized compound was ensured by specific recrystallization. Reaction yield: 53 %. ESI-MS (positive mode, MeOH:H_2O) *m/z*: $[LNa]^+$ calculated for $C_{14}H_{13}N_5O_6Na$ 370.27, found 370.2; $[LH]^+$ calculated for $C_{14}H_{14}N_5O_6$ 348.29 found 349.0.

*Pyridoxal-3-hydroxybenzoic acid hydrazone (**3**)*

Compound **3** was obtained with good yield by condensation of pyridoxal hydrochloride with 3-hydroxybenzoic acid hydrazide. A solution of 0.152 g (1 mmol) of 3-hydroxybenzoic acid hydrazide in methanol (5 mL) was prepared. Parallelly, 0.204 g (1 mmol) of pyridoxal hydrochloride was dissolved in the same solvent (5 mL). The resulting solution was added slowly to the hydrazide under constant stirring. To the obtained pale-yellow mixture were added few drops of glacial acetic acid. The mixture was stirred at 60 °C for 4 h until its colour changed to intense yellow. Further, it was concentrated to half of the initial volume when the fine yellow mass was formed. The resulting solid compound was filtered, washed with alcohol and dried under vacuum. Reaction yield: 71 %. ESI-MS (positive mode, MeOH:H_2O) *m/z*: $[LNa]^+$ calculated for $C_{15}H_{15}N_3O_4Na$ 324.3, found 324.2.

*Pyridoxal-4-phenyl-3-thiosemicarbazone (**4**)*

Compound **4** was prepared following the method described by Manikandan et al. [28]. To a solution of 0.204 g (1 mmol) of pyridoxal hydrochloride in methanol (10 mL) was added dropwise a solution of 0.167 g (1 mmol) 4-phenyl-3-thiosemicarbazide dissolved in the minimum amount of alcohol (5 mL). The yellow solution was refluxed for 2 h. After concentrating the solution and cooling at 4 °C, a yellow solid mass was isolated and purified by recrystallization. Reaction yield: 67 %. ESI-MS (positive mode, MeOH:H_2O) *m/z*: $[LH]^+$ calculated for $C_{15}H_{17}N_4O_2S$ 317.3, found 317.2.

*Pyridoxal-4-benzyl-3-thiosemicarbazone (**5**)*

This compound was synthesized in a similar manner as the previous one. A solution of 0.204 g (1 mmol) of pyridoxal hydrochloride in methanol (5 mL) was prepared. Separately, 0.181 g (1 mmol) of 4-benzyl-3-thiosemicarbazide was dissolved in 5 mL methanol and added to the first solution. The resulting mixture was refluxed at controlled temperature for 2 h until a light yellow precipitate was obtained. Afterwards, it was collected, purified and dried. Reaction yield: 73 %. ESI-MS (positive mode, MeOH:H_2O) *m/z*: $[LH]^+$ calculated for $C_{16}H_{19}N_4O_2S$ 331.4, found 331.1.

*N-(4-amino-1,5-dimethyl-2-phenyl-1,2-dihydro-3H-pyrazol-3-one)-4-acetoxy-3-methoxybenzaldimine (**6**)*

A solution of 4-aminoantipyrine (0.203 g, 1 mmol) in chloroform (5 mL) was prepared and added to a solution of 4-acetoxy-3-methoxybenzaldehyde (0.194 g, 1 mmol) in methanol (5 mL). The mixture was stirred under controlled temperature for 2 h. Afterwards, the solution was left to cool at room temperature and slowly evaporated until a light yellow solid precipitate was formed. In order to obtain the single crystals suitable for X-ray diffraction, a small amount of finished compound was re-dissolved in a chloroform:methanol (1:1, v/v) mixture and kept at 4 °C. After few days, fine crystals were isolated. Reaction yield: 48 %. ESI-MS (positive mode, MeOH:H_2O) *m/z*: $[LH]^+$ calculated for $C_{21}H_{22}N_3O_4$ 380.4, found 380.1.

Compounds (7) and (8) were obtained in a similar way as compound (6)

*N-(4-amino-1,5-dimethyl-2-phenyl-1,2-dihydro-3H-pyrazol-3-one)-3-benzyloxy-4-methoxybenzaldimine **(7)***

A solution of 0.242 g (1 mmol) of 3-benzyloxy-4-methoxybenzaldehyde in methanol (5 mL) was added to the solution of 0.203 g (1 mmol) 4-aminoantipyrine dissolved in minimum volume of chloroform (5 mL). The mixture was stirred for 2 h and afterwards left to cool at room temperature. After 30 min, fine light yellow precipitate appeared. Afterwards, it was filtered and washed with alcohol. Reaction yield: 80 %. ESI-MS (positive mode, MeOH:H_2O) *m/z*: $[LNa]^+$ calculated for $C_{26}H_{25}N_3O_3Na$ 450.4, found 450.2; $[LH]^+$ calculated for $C_{26}H_{26}N_3O_3$ 428.5, found 428.3.

*N-(4-amino-1,5-dimethyl-2-phenyl-1,2-dihydro-3H-pyrazol-3-one)-4-(dimethylamino)benzaldimine **(8)***

A solution of 4-aminoantipyrine (0.203 g, 1 mmol) in chloroform (5 mL) was prepared and added to a solution of 4-(dimethylamino)benzaldehyde (0.149 g, 1 mmol) in the same solvent (5 mL). The final mixture was stirred at room temperature for 4 h. After concentrating the mixture, a shiny orange polycrystalline powder was isolated. To obtain X-ray single-crystals, a certain amount of compound was dissolved in 3 mL of methanol in a tube. The same volume of acetone was slowly added on the tube walls. The tube was left at 4 °C for few days when crystals were separated from the solution. Reaction yield: 64 %. ESI-MS (positive mode, MeOH:H_2O) *m/z*: $[LNa]^+$ calculated for $C_{20}H_{22}N_4ONa$ 357.4, found 357.2; $[LH]^+$ calculated for $C_{20}H_{23}N_4O$ 335.4, found 335.2.

Analysis/techniques

The percentages of C, H and N were determined by elemental analysis using a Carlo-Erba microdosimeter. All compounds were dried prior analysis at 100 °C. The IR spectra were measured by using KBr pelletizing technique and registered with a BioRad FTS 135 spectrophotometer in the region 600–4000 cm^{-1}. The ^1H and ^{13}C NMR spectra were recorded with a Bruker DRX 400 spectrometer, at room temperature. Chemical shifts were measured in parts per million using standard tetramethylsilane (TMS). Solutions of compounds in deuterated dimethylsulfoxide (DMSO) were used for testing. Mass spectra were obtained with a tandem mass spectrometer operated in MS mode (mass range of 5–500 *m/z*). Samples were delivered via infusion into the electrospray probe. For testing purposes, each compound was dissolved in methanol:water mixture and injected directly into the mass spectrometer's interface. The determination of thermal stability of compounds was accomplished by non-isothermal chemiluminescence in static air atmosphere at three heating rates: 5, 10 and 15 °C min^{-1}. The equipment, LUMIPOL 3, was manufactured by Institute of Polymers, Slovak Academy of Sciences. Because the evolution of emission intensities follows the accumulation of carbonyl intermediates [29], this procedure depicts the progress in the oxidation state of investigated material. The error of temperature measurements on the oven is ±0.5 °C. Powder samples of around 3 mg were placed in an aluminium crucible after pre-weighting. For reliable comparison, the chemiluminescence intensities were normalized to unit mass, the results being expressed in Hz g^{-1}, which represent the number of photons emitted by 1 g of sample. The listed intensity values are the sums of counted photons over 1 min divided by 60 for their conversion in Hz (counts per second). Differential scanning calorimetry (DSC) measurements were performed using a Setaram 131 EVO (Setaram Instrumentation, France), in the following conditions: temperature range, 30–350 °C; heating rate, 10 K min^{-1}; atmosphere, air (gas flow, 50 mL min^{-1}). Samples of about 2–3 mg of ligands powder were measured in aluminium pans of 30 μL. Specific SETARAM software has been used for data acquisition and processing. Different parameters characterizing the observed effects (peaks), such as the oxidation onset temperature (OOT), the peak temperature (T_m) or the thermal effect (ΔH), were calculated from the DSC curves. Thermo-gravimetric study was performed with an Equipment STA 449 Jupiter, using crucibles of sinterized Al_2O_3, in dynamical atmosphere composed by a flow of 13 mL min^{-1} oxygen and a flow of 37 mL min^{-1} nitrogen in sample furnaces. Temperature program was identical in all the cases, from room temperature 25–350 °C with a heating rate of 10 °C min^{-1}.

X-ray diffraction studies

Crystallographic measurements were carried out with an Oxford-Diffraction XCALIBUR E CCD diffractometer equipped with graphite-monochromated Mo-Kα radiation. Single crystals were positioned at 40 mm from the detector, and 309 and 405 frames were measured each for 30 and 5 s over 1° scan width for **6** and **8**, respectively. The unit-cell determination and data integration were carried out using the CrysAlis package of Oxford Diffraction [30]. The structures were solved by direct methods using Olex2 [31] software with the SHELXS structure solution program and refined by full-matrix least-squares on F^2 with SHELXL-97 [32]. Atomic displacements for non-hydrogen atoms were refined using an anisotropic model. All hydrogen atoms were refined as riding on their carriers with

$U_{iso}(H) = 1.2_{eq}$ (CH,) and $U_{iso}(H) = 1.5_{eq}$ (CH3). Using the Olex2 [31] program, the molecular plots were obtained. The main crystallographic data together with refinement details are summarized in Table 1. CCDC 1440749 (for compound **6**) and CCDC 1440723 (for compound **8**) contain the supplementary crystallographic data for this contribution. These data can be obtained free of charge via www.ccdc.cam.ac.uk/conts/retrieving.html (or from the Cambridge Crystallographic Data Centre, 12 Union Road, Cambridge CB2 1EZ, UK; fax: (+44) 1223-336-033; or deposit@ccdc.ca.ac.uk).

Results and discussion

The general approach for the preparation of the azomethine compounds involves the condensation reaction between the carbonyl group of a molecule and a second reagent containing an amine function. The nature of the aminic reagent induces wide variation of the electronic and steric properties of the final condensation product [5, 22]. The study described here concerns three different types of azomethine compounds—hydrazones, thiosemicarbazones and Schiff bases. Although all these compounds possess as common element the –C=N bond, they differ by the nature of the donor atoms in the proximity of the imine site. The structures of compounds **1**–**8** are presented in Fig. 1. The molecular formula for each compound was confirmed by elemental analysis, and the results are indicated in Table 2. In addition, the molecular mass was confirmed by the ESI-MS spectra. ESI is as a mild ionization method which allows the capture of the molecular ion. In this way, valuable information about the molecular mass of the azomethine compounds was obtained. The ESI-MS spectra of compounds **1**, **4**, **5** and **6** exhibit intense peak corresponding to $[LH]^+$ ion at 259.0, 317.2, 331.1 and 380.1 Da,

Table 1 Crystallographic data, details of data collection and structure refinement parameters for **6** and **8**

	6	**8**
Empirical formula	$C_{21}H_{21}N_3O_4$	$C_{20}H_{22}N_4O$
Formula mass	379.41	334.42
Temperature/K	173(2)	173.00(10)
Crystal system	Triclinic	monoclinic
Space group	$P-1$	C2/c
a/Å	7.0352(5)	17.8014(16)
b/Å	9.7036(6)	6.8034(6)
c/Å	14.4466(18)	29.535(3)
α/°	96.406(7)	90.00
β/°	100.351(8)	101.368(9)
γ/°	102.956(6)	90.00
V/Å^3	933.55(14)	3506.8(5)
Z	2	8
D_{calc}/mg mm^{-3}	1.350	1.267
μ/mm^{-1}	0.095	0.081
Crystal size/mm^3	0.40 × 0.15 × 0.15	0.60 × 0.20 × 0.20
θ_{min}, θ_{max}/°	2.9 to 50.04	4.66 to 50.04
Reflections collected	6956	11,871
Independent reflections	3295 [R_{int} = 0.0333]	3086 [R_{int} = 0.0535]
Data/restraints/parameters	3295/0/257	3086/0/230
$R_1^a(I > 2\sigma(I))$	0.0503	0.0461
wR_2^b (all data)	0.1233	0.1132
GOF[c]	1.022	1.065
Largest diff. peak/hole/e Å^{-3}	0.26/−0.24	0.18/−0.19

[a] $R_1 = \Sigma||F_o| - |F_c||/\Sigma|F_o|$

[b] $wR_2 = \{\Sigma[w\ (F_o^2 - F_c^2)^2]/\Sigma[w(F_o^2)^2]\}^{1/2}$

[c] GOF = $\{\Sigma[w(F_o^2 - F_c^2)^2]/(n-p)\}^{1/2}$, where *n* is the number of reflections and *p* is the total number of parameters refined

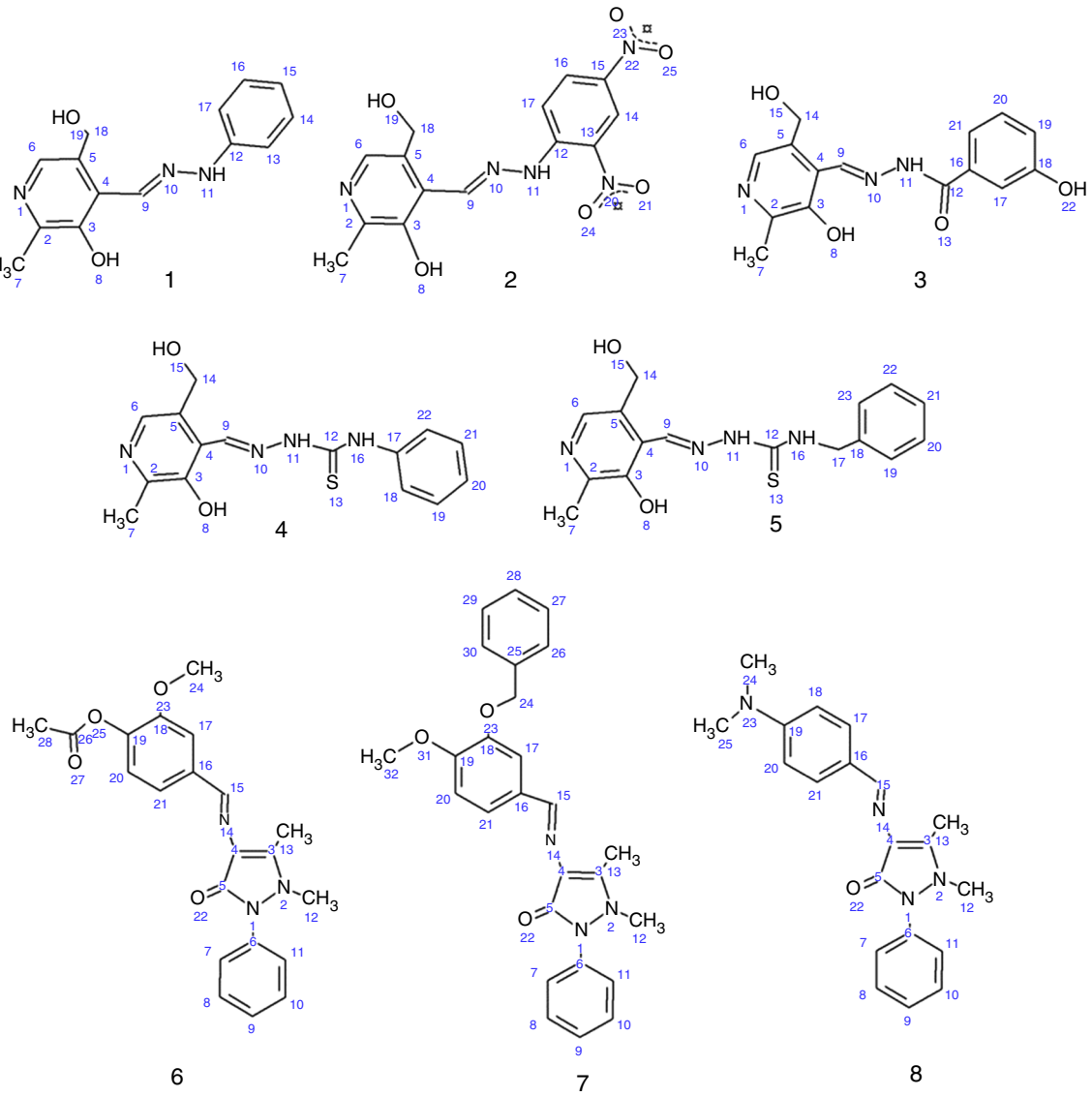

Fig. 1 Structures of compounds **1–8**

Table 2 Elemental analysis results for compounds **1–8**

Compound	Molecular formula	Found/%			Calculated/%		
		C	H	N	C	H	N
1	$C_{14}H_{15}N_3O_2$	66.12	5.69	15.85	65.37	5.83	16.34
2	$C_{14}H_{13}N_5O_6$	47.80	3.61	20.65	48.41	3.75	20.17
3	$C_{15}H_{15}N_3O_4$	58.95	4.89	14.18	59.80	4.98	13.95
4	$C_{15}H_{16}N_4O_2S$	57.21	4.98	17.43	56.96	5.06	17.72
5	$C_{16}H_{18}N_4O_2S$	58.30	5.92	16.33	58.18	5.45	16.96
6	$C_{21}H_{21}N_3O_4$	66.21	6.06	10.54	66.49	5.54	11.08
7	$C_{26}H_{25}N_3O_3$	72.74	6.07	9.22	73.06	5.85	9.83
8	$C_{20}H_{22}N_4O$	71.24	7.46	16.91	71.85	6.58	16.77

respectively. In case of compounds **2**, **3**, **7** and **8,** the formation of Na adducts is shown by the peaks recorded at 349.0, 324.2, 450.2 and 357.2 Da, respectively.

The described compounds can serve as excellent ligands for the preparation of metal complexes. Based on the number and position of the heteroatoms, chelate rings characterized by different dimension and stability can be obtained.

X-ray diffraction

The results of single-crystal X-ray study for compounds **6** and **8** along with the atom numbering scheme are shown in Figs. 2a and 3a, while the interatomic distances and angles are summarized in Table 3—supplementary documents. The crystals of **6** and **8** have a molecular structure built up from the corresponding neutral entities without any solvate molecules in the asymmetric part. The studied compounds exhibit similar structures with closed geometric parameters (Table 1A—supplementary documents) comprising a planar fragment formed by pyrazole and benzaldimine moieties (dihedral angles 1.06°, 8.64° for **6** and **8**, respectively) and twisted phenyl substituent (dihedral angles 56.16° and 51.11° for **6** and **8**, respectively). In compound **6**, the acetate group is nearly perpendicular to the aromatic ring (dihedral angle 73.46°). The main crystal structure motif for compounds **6** and **8** is characterized as one-dimensional supramolecular architecture, based on the formation of C–H···O intermolecular hydrogen bonds. A view of these architectures along with the H-bonds parameters for compounds **6** and **8** is shown in Fig. 2b and Fig. 3b, respectively. Significant stacking interactions in the crystal structure **6** (centroid-to-centroid distance 3.519 Å) and C–H···π interactions (2.729 Å) in **8** are also present.

IR spectra

The signals in the IR spectra have been assigned to the vibration of the main bonds and fragments in the azomethine molecules. The lack of bands characteristic to the carbonyl and amine groups in the spectra of azomethine compounds confirm the condensation reaction took place. Instead, a new well-defined band appears in the region 1590–1630 cm^{-1}. This is a typical signal for the vibration of the C=N bond [33]. The infrared spectra of compounds **1** and **2** are similar. Both of them emphasize the specific signal ν(C=N) at 1601 cm^{-1} and 1608 cm^{-1}, respectively. The broad signal at 3270–3430 cm^{-1} is assigned to the hydroxyl group. A sharp signal at 1245 cm^{-1} and 1217 cm^{-1}, respectively, is characteristic to the vibration of the –OH group attached to the pyridine ring in the pyridoxal moiety. Another similar signal can be observed at lower frequencies (1068 cm^{-1} and 1035 cm^{-1}), this one being characteristic to the $–CH_2$-OH group [33]. Lastly, the broad band visible at high frequencies suggests the establishment of intra-molecular interactions via hydrogen bond, possible due to the hydroxyl groups and = N–N-group. The spectra of compound **3** exhibit similar signals as described above. In addition, the presence of the –HC=N–NH–C=O group is emphasized by a series of specific signals between 1047 and 1685 cm^{-1}. Because of this fragment, the hydrazone molecule is subjected to keto–enol equilibrium phenomena (Fig. 4a). The decision on the stabilized tautomeric form was made based on the infrared spectra analysis and

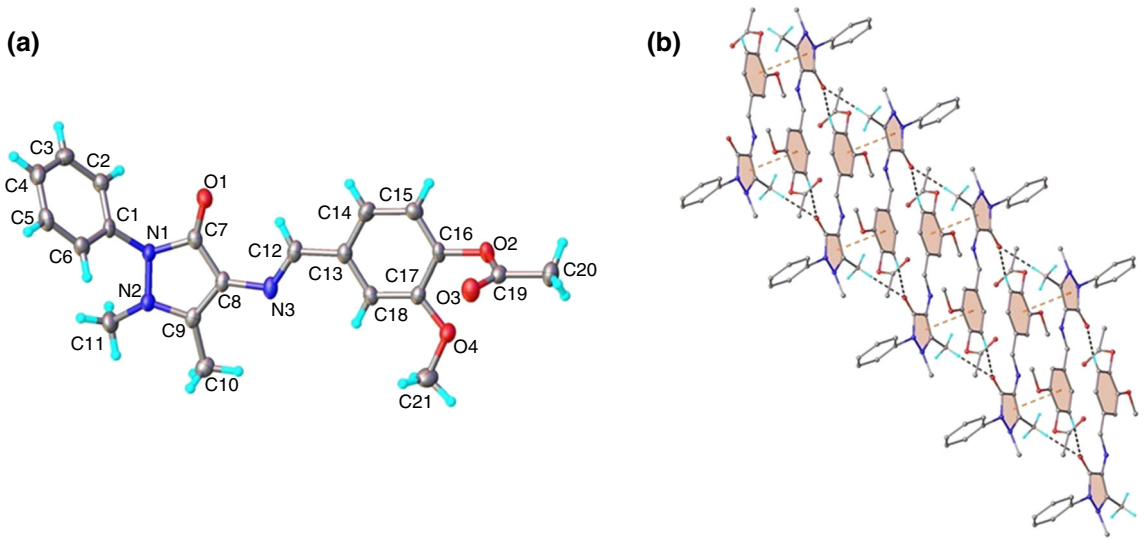

Fig. 2 **a** X-ray molecular structure of **6**. Thermal ellipsoids are drawn at 50 % probability level; **b** one-dimensional supramolecular architecture in the crystal structure of **6**. H-bonds parameters: C10-H···O1 [O10−H 0.96 Å, H···O1(1 + *x*, *y*, *z*) 2.433 Å, C10···O1 3.393(4) Å, C10−H···O1 178.5°]; C15-H···O1 [O10−H 0.93 Å, H···O1(−*x*, −*y*, −*z*) 2.392 Å, C15···O1 3.272 (4) Å, C10−H···O1 157.9°]

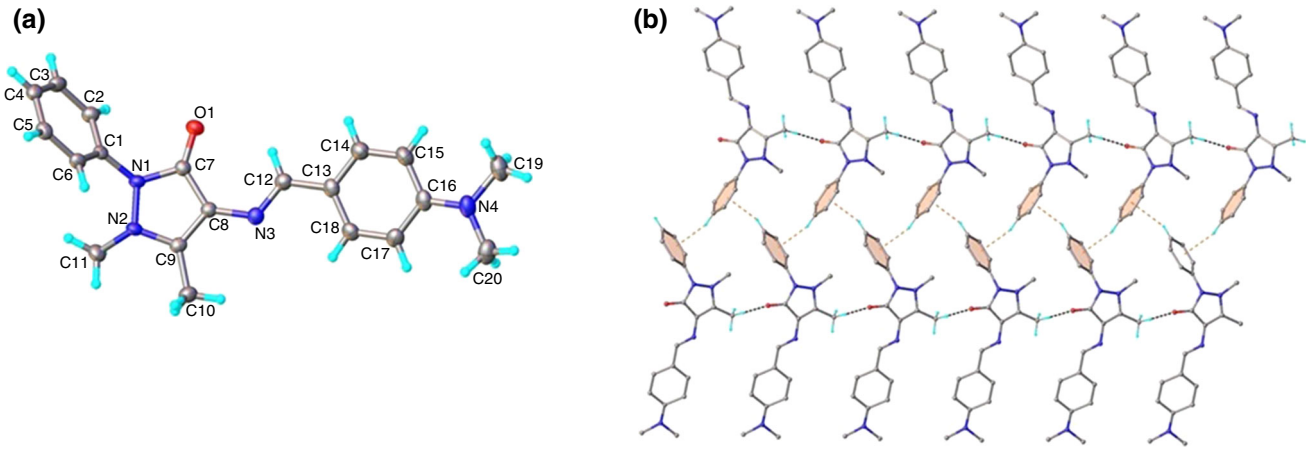

Fig. 3 **a** X-ray molecular structure of **8**. Thermal ellipsoids are drawn at 50 % probability level. **b** One-dimensional supramolecular architecture in the crystal structure of **8**. H-bond parameters: C10–H···O1 [O10–H 0.96 Å, H···O1(x, $-1 + y$, z) 2.405 Å, C10···O1 3.357(4) Å, C10–H···O1 171.5°]

pertinent bibliographical references [34, 35]. The medium signal recorded at 1685 cm^{-1} represents the effect of the stretching vibration of the –C=O and C–N bonds (amide I band). Moreover, the IR spectra exhibits two additional signals which are characteristic to the N–C=O stretching vibration at 1546 cm^{-1} (amide II) and C–N stretching vibration coupled with NH bending effect at 1349 cm^{-1} (amide III). These signals suggest the stabilization of the keto tautomeric form. The presence of the hydroxyl group bonded to the pyridine ring could induce the possibility of a third tautomeric form in which this hydroxyl group is converted into a keto one. Still, this hypothesis is not confirmed by the IR spectra as the presence of the OH group is clearly emphasized by the signal recorded at 1211 cm^{-1}. The vibration spectra of compounds **4** and **5** are similar and exhibit the main expected signals for the desired thiosemicarbazones. The formation of the imines is proven by the bands associated with the azomethine bond at 1622 and 1630 cm^{-1}, respectively. Also, the presence of the aryl-hydroxy group is emphasized by the signal at 1221 and 1274 cm^{-1}, respectively. In case of thiosemicarbazones, the thiol–thione equilibrium is frequently encountered and can lead to different forms in microcrystalline powder and liquid phase [36, 37] (Fig. 4b). The thione form of the compounds **4** and **5** was determined based on IR and NMR spectra assessment. The IR spectra of the compound **4** exhibit the band characteristic to ν(C=S+C=N) vibration at 1302 cm^{-1}, as well as a sharp signal at 756 cm^{-1} assignable to the C=S bond stretching [33]. Another important signal observed at 1554 cm^{-1} is the one associated to the N–C=S stretching vibration mode which confirms the thione form. Compound **5** describes a similar pattern with the target bands recorded at 1325 cm^{-1} (ν(C=S+C=N)), 817 cm^{-1} (ν(C=S)) and 1560 cm^{-1} (ν(N–C=S)). The IR spectra of compound **6**, **7** and **8** show the signals specific to the main groups in the 4-aminoantipyrine and carbonyl molecules. The conversion of the reagents is clearly indicated by the medium band recorded at 1591 cm^{-1} (**6**), 1594 cm^{-1} (**7**) and 1609 cm^{-1} (**8**) assigned to ν(C=N). The signals at 1635 cm^{-1} (**6**), 1638 cm^{-1} (**7**) and 1643 cm^{-1} (**8**) correspond to the keto exocyclic group attached to the pyrazole ring. In case of compound **6,** a special issue is encountered due to the presence of the C=O bond originating from the acetate fragment. This fragment is represented in the IR spectra by the sharp band at the higher frequency—1766 cm^{-1} [33]. The correct assignment of this band versus the one associated to the C=O exocyclic one is important in view of the

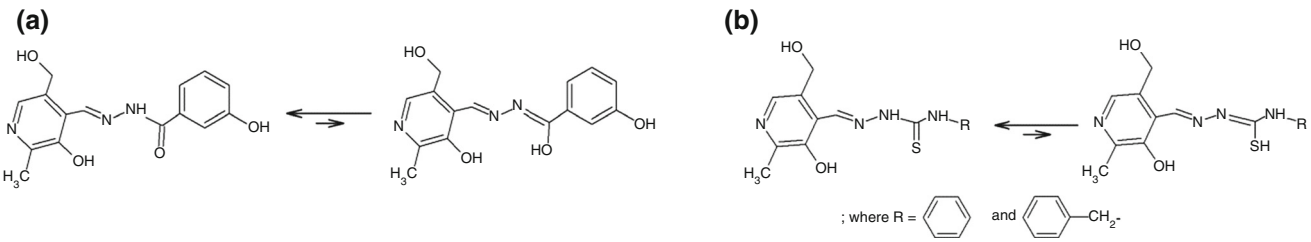

Fig. 4 **a** Tautomeric equilibrium for compound **3**; **b** tautomeric equilibrium for compounds **4** and **5**

potential coordination properties of the organic molecule to transition metal ions and the correct interpretation of the complex structure.

^{1}H and ^{13}C NMR spectra

All the compounds were characterized by means of NMR spectroscopy in order to confirm the proposed molecular structures. In addition, the NMR spectra data provide helpful information about the tautomeric equilibrium in solution and about the most stable conformation adopted by the organic molecules. The main ^{1}H NMR and ^{13}C NMR signals are indicated in *Supplementary documents*.

The ^{1}H NMR spectra of compounds **1** and **2** display a pattern of similar signals. The singlets recorded at δ 2.6 ppm and δ 4.76–4.86 ppm correspond to methyl and methylene groups attached to the pyridine ring. This data are confirmed also by the signals identified in the ^{13}C NMR spectra at δ 38.60–38.67 ppm and δ 58.88–59.17 ppm, respectively. The region between 6.25 and 8.45 ppm shows a series of multiplets characteristic to the protons of the aromatic rings. Valuable information about the molecules fragments containing heteroatoms was obtained by analysing the high region of the ^{1}H NMR spectra. The resonance at δ 8.17 ppm (compound **1**) and δ 8.90 ppm (compound **2**) is assigned to the azomethine bond proton. The presence of the imine hydrogen is described also by the signals at δ 142.64 ppm and δ 144.03 ppm in the ^{13}C NMR spectra. The signals observed in the ^{1}H NMR spectra of compound **1** at δ 8.40 ppm and at δ 9.16 ppm in the spectra of compound **2** are associated to the aryl –OH groups in the pyridoxal moiety. The signal at highest resonance can be attributed to the –N–H proton. The shift of this peak at resonance energies close to δ 12 ppm indicates the interaction of the organic compounds with neighbour solvent molecules via hydrogen bonds. These data are in accord with previously reported ones about other hydrazones [38]. The assignment of the signals in the NMR spectra of compound **3**, **4** and **5** is more complex in view of multiple intermolecular interactions and conformation stabilization. The formation of the azomethine bond is confirmed by the signals at δ 8.19–8.65 ppm in the ^{1}H NMR spectra and the one at δ 142.75–143.83 ppm in the ^{13}C NMR spectra. The keto, respectively, thione form suggested also by the IR spectra is confirmed by the presence of the signal at δ 9.25–10.62 ppm in the ^{1}H NMR spectra characteristic to the –N–H proton in the amide/thiosemicarbazide fragment in E conformation [39]. For compound **3,** the same conclusion is supported by the C=O typical signal observed at δ 163.24 ppm in the ^{13}C NMR spectra. In case of compounds **4** and **5,** the stabilization of the thione form is proven by the signal at δ 177–179 ppm characteristic to the C=S bond. The complete assignment of the signals in the NMR spectra of compounds **6**, **7** and **8** is more difficult due to the complexity of the molecules. COSY technique was helpful for the determination of the spins which are coupled to each other. The signals specific to the azomethine fragment (δ 9.58–9.71 ppm in the ^{1}H NMR spectra and δ 148.44–152.06 ppm in the ^{13}C NMR spectra) are the proof of the Schiff base formation. Moreover, the signal between δ 158.05–161.06 ppm in the ^{13}C NMR spectra is associated to the carbon involved in the C=O exocyclic group from the 4-aminoantipyrine moiety.

Chemiluminescence studies

The thermal stability of inorganic complexes is depicted by the bonding strength of ligands [40], but the decomposition of these constitutive moieties brings an important effect on the material integrity over time or temperature ranges. The chemical structure, the electronic interactions between various segments of ligands, the existence environment or the operation temperature can influence the thermal stability. The electronic effects of substituents in the benzene rings of the structures are the consequence of electronic influence on the N–N bridges. The donating or withdrawing character of substituents modifies the charge distribution inside the molecules of azomethine-type compounds. The presence of pyrazole configuration gets supplementary contribution to the variation in the stability of studied molecules.

The onset oxidation temperatures (OOT) for compounds **1**–**3** indicate a lower thermal stability of the hydrazone-type molecules.

In Fig. 5, the compound **4**, whose structure contains slightly polarized thio-ketone group, presents one intensity maximum at 205 °C, which is the consequence of the early start of oxidation. The ligand **5**, which possesses the same group, is suddenly oxidized at 225 °C. The similar results were recorded at higher heating rates, when amplified CL intensities were noticed. The change in the heating rate caused the modification in the emission intensities of ligands, which can be ascribed to the vulnerability of molecules during oxidation. The difference in the thermal stability of the studied structures may be also ascribed to the hydrogen bonds established between protons and atoms with available electrons concerning especially oxygen atoms. The highest heating rate (β = 15 °C min^{-1}) have not distinguished behaviour in comparison with the lower heating conditions (Fig. 1A—supplementary documents).

The OOT (Table 3) and the profiles of CL intensity dependences on temperatures (Figs. 5, 6 and Fig. 1A—see supplementary data) depict the contribution of molecular configurations to the progress of degradation, when the substituents have different positions and the sterical hindrance modifies the distribution of more reactive sites. The

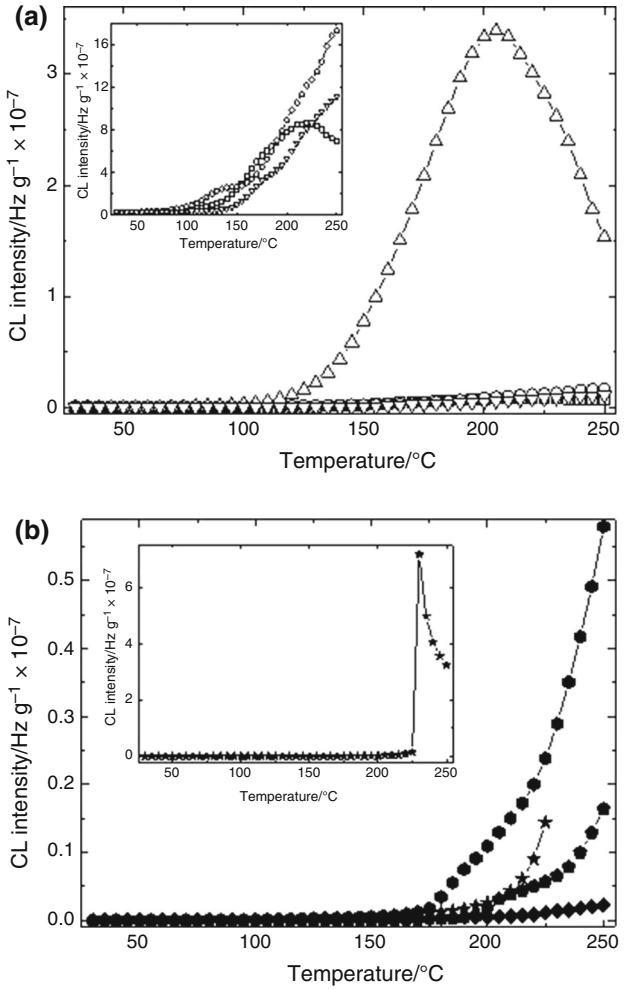

Fig. 5 Non-isothermal CL spectra recorded on the samples **a 1–4** and **b 5–8** at the heating rate of 5 °C min^{-1}

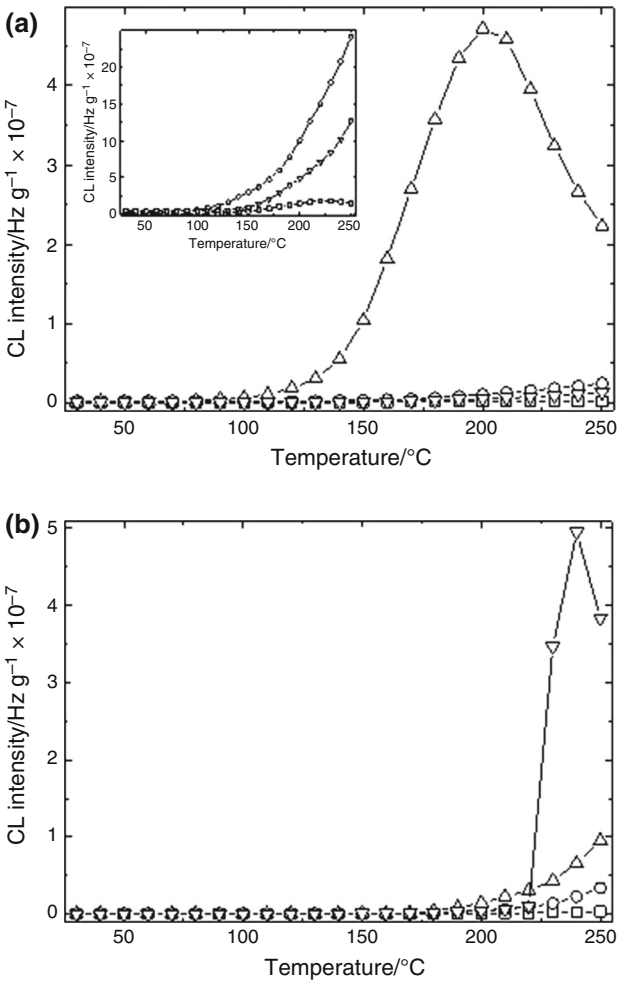

Fig. 6 Non-isothermal CL spectra recorded on the samples **a 1–4** and **b 5–8** at the heating rate of 10 °C min^{-1}

benzene rings, which have a well-defined electronic homogeneity, are the supports of chemical interactions through which certain bonds are weakened. The pyrazole structure existing in the configurations **6–8** can be considered a weaker fragment, where oxidation can start by bond cleavage.

The components of two groups differ by the real development of oxidation state. While compounds **1–4** have smaller onset oxidation temperature, the structures **6–**

Table 3 Onset oxidation temperatures for compounds **1–8**

Compound	Onset oxidation temperature/°C		
	β = 5 °C min^{-1}	β = 10 °C min^{-1}	β = 15 °C min^{-1}
1	135	148	163
2	150	153	158
3	142	148	153
4	155	158	168
5	202	210	215
6	211	220	228
7	210	215	222
8	215	219	224

Table 4 DSC and TG parameters for compounds **1–8**

Compound	*OOT*/°C	ΔH_{ox}/J g^{-1}	T_{max}/°C	T_m/°C	ΔH_m/J g^{-1}	Mass loss/%
1	245	−170	266	–	–	11
2	266	−582	267	–	–	50
3	214	−169	273	–	–	30
4	218	−45	239	–	–	22
5	201	−42	215	–	–	23
6	284	−83	321	173	307	51
7	301	−401	325	167	68	41
8	287	−217	320	221	221	65

8 present a slight change in the CL intensities as testing temperature increases (Fig. 2A—supplementary documents). The higher thermal stability of compounds **6–8** recommends these structures as the most proper ligands from the studied series for complexes design.

Thermal analysis studies

The results of the thermal analysis provide a comprehensive picture of the thermal degradation process and enable the calculation of specific thermodynamic parameters. The values of OOT, oxidation enthalpy (ΔH_{ox}), maximum temperature of the oxidation peak (T_{max}) as well as melting temperature (T_m) and melting enthalpy (ΔH_m) for compounds **6–8** are provided in Table 4.

The thermal oxidation stability of the compounds is strongly connected with their structure. The values of the OOT parameter show that all the molecules present a good stability to oxidation, higher than 200 °C. The stability of the compounds decreases in the following direction:

Compound **7** > Compound **8** > Compound **6** > Compound **2** > Compound **1** > Compound **4** > Compound **3** > Compound **5**

The DSC curves for compounds **1** and **3** (Fig. 7) are similar. In case of **1**, the lower temperature region of the curve presents three small endothermal peaks at about 87 °C (8.4 J g^{-1}), 104 °C (3.1 J g^{-1}) and 121 °C (1.4 J g^{-1}), respectively. As observed from TG/DTG curves (Fig. 3A—supplementary documents), these endothermal peaks are not being accompanied by a noticeable mass loss.

The curve of compound **3** describes also three endothermal degradation steps with peaks at 96 °C (7.5 J g^{-1}), 137 °C (21.1 J g^{-1}) and 153 °C (57.8 J g^{-1}), respectively. The TG analysis (Fig. 4A—supplementary

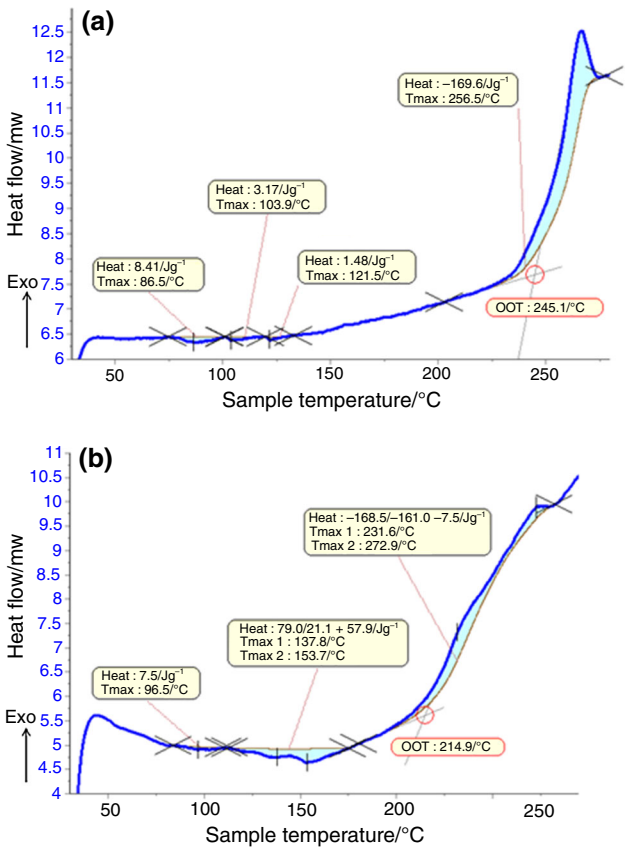

Fig. 7 DSC curves for **a 1** and **b 3**

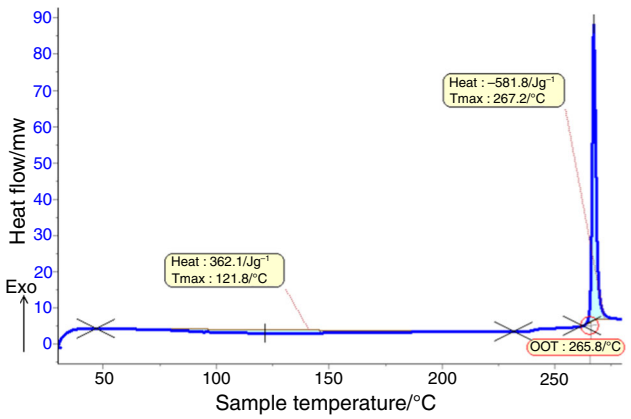

Fig. 8 DSC curve for compound **2**

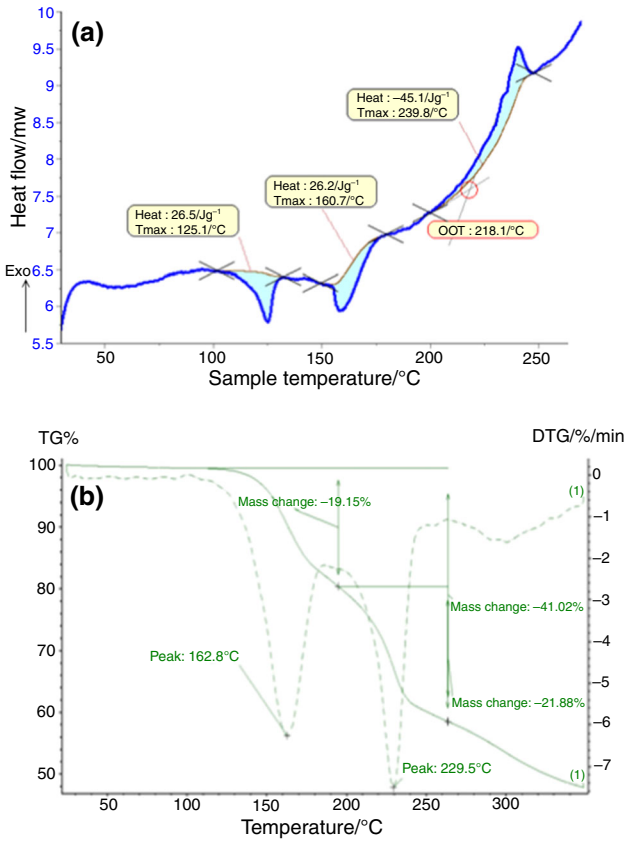

Fig. 9 DSC (**a**) and TG (**b**) curves for compound **4**

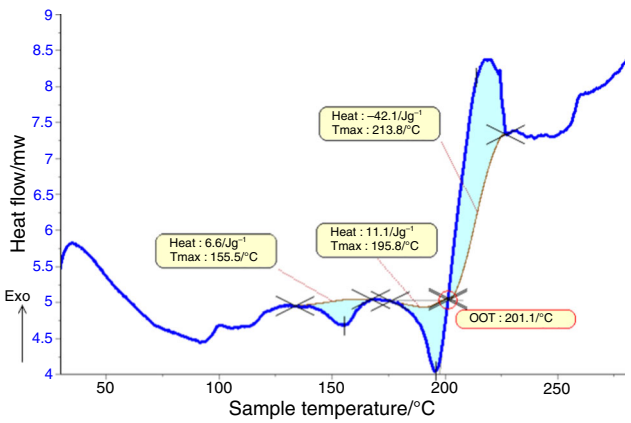

Fig. 10 DSC curve for compound **5**

documents) presented a total mass loss of about 5 %, and these endothermal effects could be associated with the evaporation of some water molecules or volatile compounds [41].

The DSC curve of compound **2** exhibits a single, large endothermal peak with a maximum at 121 °C assigned to the evaporation of water molecules (Fig. 8). This finding is supported also by the TG/DTG analysis results (Fig. 5A—supplementary documents). The oxidation step is associated with a mass loss of approximately 50 % of the initial mass. For compound **4,** the DSC curve displays two endothermal peaks at 125 °C (26.5 J g^{-1}) and 161 °C (26.3 J g^{-1}) (Fig. 9a). The first endothermal peak could be assigned to the melting of some crystalline domains, not being accompanied by a mass loss, while the second peak presents a mass loss of about 19 % due to, probably, the evaporation of volatile molecules (Fig. 9b) [41]. The DSC curve of compound **5** also presents two endothermal peaks, but at higher temperatures: 155 °C (6.6 J g^{-1}) and 195 °C (11.1 J g^{-1}). The last peak could be assigned to a little

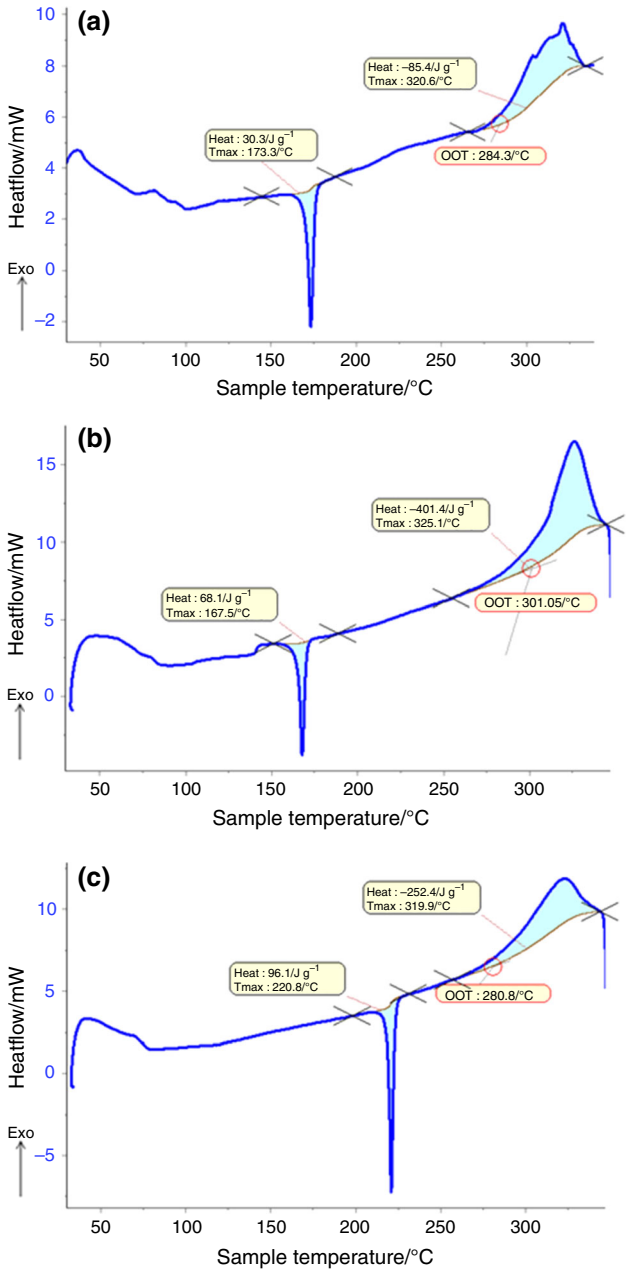

Fig. 11 DSC curves for **6** (**a**), **7** (**b**) and **8** (**c**)

decomposition of the compound followed by the oxidation process (Fig. 10). The mass loss generated by the oxidation process represents 23 % of the initial mass (Fig. 6A—supplementary documents).

The DSC curves recorded on compounds **6–8** are similar and undertake an endothermal process before oxidation represented by the peaks at about 173 °C (**6**, 307 J g^{-1}), 167.5 °C (**7**, 68.1 J g^{-1}) and 221 °C (**8**, 92 J g^{-1}), respectively (Fig. 11). These peaks are due to the melting of the crystalline structure of the analysed samples. These results are well correlated with the TG/DTG data (Figs. 7A, 8A, 9A—supplementary documents). In case of each compound, the oxidation process generates a specific mass loss: 51 % (**6**), 41 % (**7**) and 65 % (**8**). From the values of the melting enthalpy, the crystallinity degree of the compounds can be estimated comparatively. The following descending trend is observed: compound **6** > compound **8** > compound **7**.

These results are in good agreement with the X-ray diffraction results based on which the molecular structures of **6** and **8** were reported.

Conclusions

The aims of this study are to describe and characterize eight azomethine-type compounds derived from pyridoxal and 4-aminoantipyrine which could be further used for the synthesis of metal complexes. The structures of the target compounds were confirmed by means of elemental analysis, IR, ^{1}H and ^{13}C NMR spectroscopy and mass spectrometry. Compounds **6** and **8** were analysed by single-crystal X-ray diffraction as well. The supramolecular motif of both organic compounds is defined by one-dimensional architecture stabilized by multiple intermolecular hydrogen bond interactions. A comprehensive thermal stability study was conducted on the basis of non-isothermal chemiluminescence at different heating rates, DSC and TG analyses. A correlation of the OOT and the molecular configuration of compounds are observed. The position of different substituents and the sterical hindrances can be identified as main molecular parameters influencing electronic charge distribution and consequently the thermal oxidation stability. In addition, the presence of intermolecular hydrogen bonds induces variations in the structure stability. All the studied compounds possess a high thermal stability with maximum of onset oxidation temperature recorded for **6–8**. In case of these molecules, the DSC curves show additional peaks associated with the melting process of the crystalline structure. This behaviour is confirmed also by the results of the TG analysis. Based on the melting enthalpy values, their crystallinity degree was evaluated showing the decreasing order: compound **6** > compound **8** > compound **7.** Due to their functional moieties and high thermal stability, these structures can be seen like suitable candidates as ligands for coordinative complexes development.

References

1. OO, Obafemi CA, Nwinyi OC, Akinpelu DA. Microwave assisted synthesis and antimicrobial activity of 2-quinoxalinone-3-hydrazone derivatives. Bioinorg Med Chem. 2010;18:214–21.
2. Aslam MAS, Mahmood SU, Shahid M, Saeed A, Iqbal J. Synthesis, biological assay and in vitro and molecular docking studies of new Schiff base derivatives as potential urease inihibitors. Eur J Med Chem. 2011;46:5473–9.
3. Cui Z, Li Y, Ling Y, et al. New class of potent antitumor acylhydrazone derivatives containing furan. Eur J Med Chem. 2010;45:5576–84.
4. Asif M, Husain A. Analgesic, anti-inflammatory and anti-platelet profil of hydrazones containing synthetic molecules. J Appl Chem: Hindawi Publishing Corporation; 2013.
5. Razaeivala M, Keypour H. Schiff base and non-Schiff base macrocyclic ligands and complexes incorporating the pyridine moiety—the first 50 years. Coord Chem Rev. 2014;280:203–53.
6. Eren T, Kose M, Kurtoglu N, Ceyhan G, McKee V, Kurtoglu M. An azo-azomethine ligand and its copper(II) complex: synthesis, X-ray crystal structure, spectral, thermal, electrochemical and photoluminescence properties. Inorg Chim Acta. 2015;430:268–79.
7. Kumar S, Nath Dhar D, Saxena PN. Application of metal complexes of Schiff bases—a review. J Sci Ind Res. 2009;68:181–7.
8. Chandra S, Gautam S, Rajor HK, Bhatia R. Synthesis, spectroscopic characterization, thermal study, molecular modeling and biological evaluation of novel Schiff's base benzil bis(5-amino-1,3,4-thiadiazole-2-thiol) with Ni(II) and Cu(II) metal complexes. Spectrochim Acta A. 2015;137:749–60.
9. Turkyilmaz M, Onder A, Baran Y. Synthesis, spectroscopic and thermal properties of some azomethine complexes of Cu(II), Ni(II) and Pt(II). J Therm Anal Calorim. 2012;109:991–8.
10. Pethe G, Yaul A, Aswar A. Synthetic, spectroscopic and thermal studies of some complexes of unsymmetrical Schiff base ligand. J Therm Anal Calorim. 2012;107:97–103.
11. Zayed EM, Zayed MA, Hindy AMM. Thermal and spectroscopic investigation of novel Schiff base, its metal complexes and their biological activities. J Therm Anal Calorim. 2014;116:391–400.
12. Labadi I, Czibulya Z, Tudose R, Costisor O. Thermal behaviour of complexes of antipyrine derivatives II. J Therm Anal Calorim. 2004;78:965–72.
13. Zaharescu T, Ilieş DC, Roşu T. Thermal and spectroscopic analysis of stabilization effect of copper complexes of EPDM. J Therm Anal Calorim. 2016;123:231–9.
14. Agarwal RK, Rastogi SC. Infrared and thermal studies of uranyl(VI) complexes of antipyrine. Thermochim Acta. 1985;95:279–81.
15. Budrugeac P, Racles C, Cozan V, Cazacu M. Thermal and thermo-oxidative stabilities of some poly(siloxane-azomethine)s. J Therm Anal Calorim. 2008;92:263–9.
16. Patrascu F, Badea M, Grecu MN, Stanica N, Marutescu L, Marinescu D, Spinu C, Tigae C, Olar R. Thermal, spectral, magnetic and antimicrobial behaviour of new Ni(II), Cu(II) and Zn(II) complexes with a hexaazamacrocyclic ligand. J Therm Anal Calorim. 2013;113:1421–9.
17. Ababei LV, Kriza A, Musuc AM, Andronescu C, Rogozea EA. Thermal behaviour and spectroscopic studies of complexes of divalent transitional metals with 2-benzoyl-pyridil-isonicotinoylhydrazone. J Therm Anal Calorim. 2010;101:987–96.

18. Abdel-Fattah HM, El-Ansary AI, Abdel-Kader NS. Thermal and spectral studies on complexes derived from tetradentate Schiff bases. J Therm Anal Calorim. 2009;96:961–9.
19. Adrover M, Vilanova B, Munoz F, Donoso J. Unexpected isomeric equilibrium in pyridoxamine Schiff bases. Bioorg Chem. 2009;37:26–32.
20. Chumnantana R, Yokochi N, Yagi T. Vitamin B6 compounds prevent the death of yeast cells due to menadione, a reactive oxygen generator. Biochim Biophys Acta. 2005;1722:84–91.
21. Mann S, Ploux O. Pyridoxal-5′-phosphate-dependente enzymes involved in biotin biosynthesis: structure, reaction mechanism and inhibition. Biochim Biophys Acta. 2011;1814:1459–66.
22. Casas JS, Couce MD, Sordo J. Coordination chemistry of vitamin B_6 and derivatives: a structural overview. Coord Chem Rev. 2012;256:3036–62.
23. Evstropol AN, Yavorovskaya VE, Vorobev ES, Khudonogova ZP, Gritsenko LN, Shmidt EV, Medvedeva SG, Filimonov VD, Prishchep TP, Saratikov AS. Synthesis and antiviral activity of antipyrine derivatives. Pharm Chem J. 1992;26:426–30.
24. Bondock S, Rabie R, Etman HA, Fadda AA. Synthesis and antimicrobial activity of some new heterocycles incorporating antipyrine moiety. Eur J Med Chem. 2008;43:2122–9.
25. Radzikowska E, Onish K, Chojak E. Prospective assessment of cancer incidence and antipyrine metabolism. Eur J Cancer. 1995;31:S225.
26. Turan-Zitouni G, Sivaci M, Kilic FS, Erol K. Synthesis of some triazolyl-antipyrine derivatives and investigation of analgesic activity. Eur J Med Chem. 2001;36:685–9.
27. Labadi I, Pal E, Tudose R, Costisor O. Thermal behaviour of complexes of antipyrine derivatives. Part III. J Therm Anal Calorim. 2006;83:681–6.
28. Manikandan R, Vijayan P, Anitha P, Prakash G, Viswanathamurthi P, Butcher RJ, Velmurugan K, Nandhakumar R. Sythesis, structure and in vitro biological activity of pyridoxal N(4)-substituted thiosemicarbazone cobalt(III) complexes. Inorg Chim Acta. 2014;421:80–90.
29. Rychly J, Matisova-Rychla L. The role of oxidation in degradation of polymers: the relation of oxidation to the light emission from oxidized polymers. Compr Anal Chem. 2008;53:451–98.
30. CrysAlis RED. Oxford Diffraction Ltd., Version 1.171.36.32; 2003.
31. Dolomanov OV, Bourhis LJ, Gildea RJ, Howard JAK, Puschmann H. *OLEX*2: a complete structure solution, refinement and analysis program. J Appl Cryst. 2009;42:339–41.
32. Sheldrick GM. A short history of *SHELX*. Acta Cryst. 2008;A64:112–22.
33. Nakamoto K. Infrared and Raman spectra of inorganic and coordination compounds. 5th ed. New York: Wiley-Interscience; 1997.
34. Manimekalai A, Saradhadevi N, Thiruvalluvar A. Molecular structures, spectral and computational studies on nicotinohydrazide. Spectrochim Acta, Part A. 2010;77:687–95.
35. Galic N, Brodanac I, Kontrec D, Miljanic S. Structural investigation of aroylhydrazones derived from nicotinic acid hydrazide in solid state and in solution. Spectrochim Acta, Part A. 2013;107:263–70.
36. Zelenin KN, Kuznetsova OB, Alekseev VV, Kalvin'Sh IY, Leitis LY. Ring-chain tautomerism of thiosemicarbazones of salicylaldehyde and pyridinecarbaldehyde in acidic media. Chem Heterocycl Compd. 1994;30:107–11.
37. Kohli E, Arora R, Kakkar R. Theoretical study of the stability of tautomers and conformers of isatin-3-thiosemicarbazone (IBT). Can Chem Trans. 2014;2:327–42.
38. Galic N, Dijanosic A, Kontrec D, Miljanic S. Structural investigation of aroylhydrazones in dimethylsulphoxide/water mixtures. Spectrochim Acta, Part A. 2012;95:347–53.
39. Despaigne AAR, da Silva JG, do Carmo ACM, Sives F, Piro OE, Castellano EE, Beraldo H. Copper(II) and Zinc(II) complexes with 2-formylpyridine-derived hydrazones. Polyhedron. 2009;28:3797–803.
40. Badea M, Olar R, Cristureanu E, Marinescu D, Emandi A, Budrugeac P, Segal E. Thermal stability study of some azo-derivatives and their complexes, Part 2. New azo-derivative pigments and their Cu(II) complexes. J Therm Anal Calorim. 2004;77:815–24.
41. Khedr AM, Marwani HM. Synthesis, spectral, thermal analyses and molecular modeling of bioactive Cu(I)-complexes with 1,3,4-thiadiazole Schiff base derivatives. Their catalytic effect on the cathodic reduction of oxygen. Int J Electrochem Sci. 2012;7:10074–93.